Institute of Mechanism Theory, Machine Dynamics and Robotics

RWTH AACHEN UNIVERSITY

This thesis was submitted to the Institute of Mechanism Theory, Machine Dynamics and Robotics

Semi-Analytical Approach - Virtual Control System Design and Loads Verification for a multi-body model of a bike

Mini-Thesis

by:
Ashutosh Mukherjee B.Sc.
Student number: 428954

supervised by:
Johannes Bolk, MSc.

Examiner:
Univ.-Prof. Dr.-Ing. Dr. h. c. Burkhard Corves
Prof. Dr.-Ing. Mathias Hüsing

Aachen, May 24, 2023

Mini-Thesis

by Ashutosh Mukherjee B.Sc.
Student number: 428954

Semi-Analytical Approach - Virtual Control System Design and Loads Verification for a multi-body model of a bike

---

The design and dimensioning of bicycles has always been a challenging task in the development process. It is necessary to resolve the conflict of objectives between a high level of safety against component failure and the requirement for a lightweight, cost-efficient design. However, determining the loads that occur during operation is a major challenge, since not all components are accessible for the application of measurement technology and the use of classical finite element methods (FEM) is often unsuitable. Already successful in the automotive and rail vehicle industry, the use of multi-body simulations (MBS) enables the link between real driving scenarios and the determination of operational loads of all system components.
In order to make the advantages of this approach available for the analysis of bicycle systems as well, this thesis will develop a method for the excitation of a digital twin based on measured data. The implementation of a control system with which imbalances in the excitation can be compensated (e.g. between handlebar and front wheel hub) offers great potential for improving the simulation. Based on preliminary work and existing concepts for implementation, the goal of the thesis is the continuation or, if necessary, new development of various solution ideas.
Possible work packages:

- Familiarization with Matlab/Simulink
- Implementation and validation of controls for stabilization of force imbalances
- Conceptual design and evaluation of alternative approaches
- Evaluation of the frame loads simulated on the bicycle based on the different simulation approaches.

Supervisor: Johannes Bolk, MSc.

Eidesstattliche Versicherung

Ashutosh Mukherjee Matrikel-Nummer: 428954

Ich versichere hiermit an Eides Statt, dass ich die vorliegende Mini-Thesis mit dem Titel

Semi-Analytical Approach - Virtual Control System Design and Loads Verification for a multi-body model of a bike

selbstständig und ohne unzulässige fremde Hilfe erbracht habe. Ich habe keine anderen als die angegebenen Quellen und Hilfsmittel benutzt. Für den Fall, dass die Arbeit zusätzlich auf einem Datenträger eingereicht wird, erkläre ich, dass die schriftliche und die elektronische Form vollständig übereinstimmen. Die Arbeit hat in gleicher oder ähnlicher Form noch keiner Prüfungsbehörde vorgelegen.

Aachen, May 24, 2023 Ashutosh Mukherjee

Belehrung:

§ 156 StGB: Falsche Versicherung an Eides Statt

Wer vor einer zur Abnahme einer Versicherung an Eides Statt zuständigen Behörde eine solche Versicherung falsch abgibt oder unter Berufung auf eine solche Versicherung falsch aussagt, wird mit Freiheitsstrafe bis zu drei Jahren oder mit Geldstrafe bestraft.

§ 161 StGB: Fahrlässiger Falscheid; fahrlässige falsche Versicherung an Eides Statt

(1) Wenn eine der in den §§ 154 bis 156 bezeichneten Handlungen aus Fahrlässigkeit begangen worden ist, so tritt Freiheitsstrafe bis zu einem Jahr oder Geldstrafe ein.

(2) Straflosigkeit tritt ein, wenn der Täter die falsche Angabe rechtzeitig berichtigt. Die Vorschriften des § 158 Abs. 2 und 3 gelten entsprechend.

Die vorstehende Belehrung habe ich zur Kenntnis genommen:

Aachen, May 24, 2023 Ashutosh Mukherjee

The present translation is for your convenience only.
Only the German version is legally binding.

Statutory Declaration in Lieu of an Oath

Ashutosh Mukherjee Student number: 428954

I hereby declare in lieu of an oath that I have completed the present Mini-Thesis entitled

Semi-Analytical Approach - Virtual Control System Design and Loads Verification for a multi-body model of a bike

independently and without illegitimate assistance from third parties. I have used no other than the specified sources and aids. In case that the thesis is additionally submitted in an electronic format, I declare that the written and electronic versions are fully identical. The thesis has not been submitted to any examination body in this, or similar, form.

Aachen, May 24, 2023 Ashutosh Mukherjee

Official Notification:

Para. 156 StGB (German Criminal Code): False Statutory Declarations

Whosoever before a public authority competent to administer statutory declarations falsely makes such a declaration or falsely testifies while referring to such a declaration shall be liable to imprisonment not exceeding three years or a fine.

Para. 161 StGB (German Criminal Code): False Statutory Declarations Due to Negligence

(1)If a person commits one of the offences listed in sections 154 to 156 negligently the penalty shall be imprisonment not exceeding one year or a fine.

(2) The offender shall be exempt from liability if he or she corrects their false testimony in time. The provisions of section 158 (2) and (3) shall apply accordingly. I have read and understood the above official notification: :

Aachen, May 24, 2023 Ashutosh Mukherjee

Contents

Formula symbols and indices

Lower case latin letters as formula symbols

n	$-$	number of simulation time-steps
$\mathbf{d}$	$-$	Vector of generalized imbalance forces
d_x	N	Net imbalance force on CF Bike along X-axis
d_y	N	Net imbalance force on CF Bike along Y-axis
d_z	N $-$ m	Net imbalance torque on CF Bike about Z-axis
$\mathbf{y}$	$-$	Vector of CF Bike CoG generalized coordinates
$\mathbf{u}$	$-$	Vector of generalized controller forces/actuation effort
u_x	N	Controller force at CF Bike CoG along X-axis
u_y	N	Controller force at CF Bike CoG along Y-axis
u_z	N $-$ m	Controller torque at CF Bike CoG about Z-axis
s	$-$	Laplace domain variable
$\mathbf{x}$	$-$	State vector
$\mathbf{r}_{FH}$	m	Moment arm of excitations on Fronthub

$\mathbf{r}_{RH}$	m	Moment arm of excitations on Rearhub
$\mathbf{r}_{H}$	m	Moment arm of excitations on Handlebar
$\mathbf{r}_{P}$	m	Moment arm of excitations on Pedals

Upper case latin letters as formula symbols

C	N	Force values from CF loadcase
R	N	Force values from RS loadcase
K	–	Feedback controller gain
$\mathbf{K}$	–	Feedback controller transfer function matrix
$\mathbf{K}_d$	–	Feedforward controller gain matrix
$\mathbf{G}$	–	Plant transfer function matrix
$\mathbf{G}_d$	–	Disturbance dynamics transfer function matrix
$\mathbf{G}_{CF}$	–	Transfer function representation of the linearized CF Bike
$\mathbf{I}$	–	Identity matrix
$\mathbf{A}$	–	System matrix

$\mathbf{B}$	–	Input matrix
$\mathbf{C}$	–	Output matrix
$\mathbf{D}$	–	Feedthrough matrix
$\mathbf{F}_{FH}$	N	Vector of excitations on Fronthub
$\mathbf{F}_{RH}$	N	Vector of excitations on Rearhub
$\mathbf{F}_{H}$	N	Vector of excitations on Handlebar
$\mathbf{F}_{P}$	N	Vector of excitations on Pedals
FX	N	Force along X-axis of inertial frame of reference
FY	N	Force along Y-axis of inertial frame of reference

Lower case greek letters as formula symbols

γ	rad	Angular position of CG Bike about the Z-axis

Indices

a	Amplitude
i	Time-step number
x	Component along X-axis
y	Component along Y-axis
z	Component along Z-axis

List of abbreviations

SAA	Semi-analytical approach
CF	Bike model for the Controlled Frame Loadcase
RS	Bike model for the Roadsurface Loadcase
MIMO	Multi-input, Multi-output
SISO	Single-input, Single-output
PD	Position-derivative control
PID	Position-integral-derivative control
MBD	Multi-Body Dynamics
FEM	Finite Element Method
RBE	Rigid Body Element
RMSE	Root Mean-Squared Error
SIMAT	Simpack Matlab S-function block for Co-Simulation
IMU	Inertial Measurement Unit
CoG	Center of gravity

1 Introduction

The most common approach of testing and validating the structural integrity and performance of bike frames and components is usually the use of test benches [FS07; Jac17]. These tests try to emulate the different kinds of loads which the bike would experience like static, dynamic and impact loads [Bru10; FS07; HHS11; Str12]. But these test benches are usually an over-simplification of the actual ride conditions, especially for mountain bikes and trail riding bikes, where the ride conditions are usually more extreme and so are the rider movements while riding the bike, which make it extremely difficult to replicate the actual loads in the test bench [Jac17; BS10; CAE16; HHS11]. Additionally, a lot of such tests are performed on individual components of the bike, but in reality during a bike ride, its components interact amongst each other and influence each other [Bru10]. An alternative is to create a digital twin, which requires faithful modelling of the rider, terrain and the bike. But for many cases, especially the ones like mountain biking or trail riding, it is extremely difficult to accurately model the manoeuvres and positions of the rider [MPR07; SM13] and the terrain-bike wheel contact [DTC13; KSM08; Red05]. A third alternative exists: *Semi-Analytical Approach* (SAA) [MX14; RTV19].

In SAA, the simulation model of only the bike is created, and to capture the rider and the terrain effects, force measurements from a real bike fitted with sensors at prescribed locations are used. The measurements recorded from the sensors are then fed to the simulation model of the bike as excitations. The workflow of SAA is illustrated in Figure 1.1.

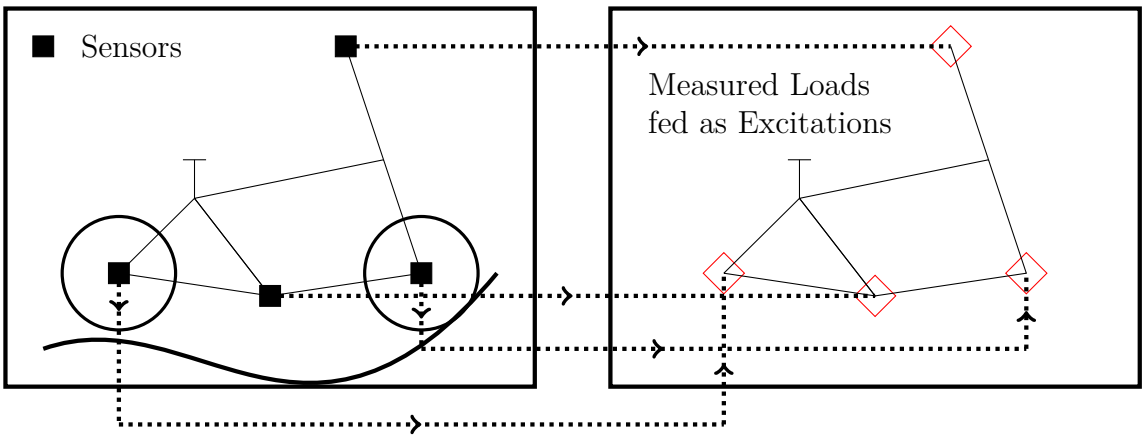

Figure 1.1: SAA Workflow

Thus, in SAA a lot of computation time and effort is saved since only the bike needs to be modelled, and the structural performance and integrity of the bike frame can be tested on the basis of the loads which will be estimated by the bike model excited by the measurements from the real bike.

2 Methodology and Concept

The prime idea behind SAA is the existence of a mathematical model of the bike, while the mathematical models of the terrain and the driver are replaced by loads measured in real-time actual riding conditions. To that end, several simulation models of the bike may be tried, each of which have to be excited by the measured loads. At the time of writing this thesis, real time sensing of loads on a real bike was still not availble, thus a reference simulation of the bike on a prescribed track is used as a proxy for the real bike fitted with sensors.

2.1 SAA Simulation Setup

The simulation set-up consists of a bike frame model, which is a simplified version of the actual bike dynamic model. There are multiple possible ways to constrain the bike frame model and different loadcases are used in order to emulate the different simulation models of the bike. In each of the loadcases, the bike frame model is the same, but the boundary conditions at the front and rear hubs are varied. For instance, in order to set-up the reference loadcase, which emulates the actual bike ride for the time being, wheels, a driver mass, a riding track and rotational degrees of freedom on the rear and front hubs are added to the bike frame model. In total, there are four loadcases being currently tested for SAA, and their nomenclature can be referred to from Figure 2.1.

The focus of this thesis is on the last loadcase i.e. the controlled frame loadcase. In this loadcase, the frame is left free in 3D space, i.e. there are no external constraints implemented on the frame. The objective in this loadcase is to implement a control system which controls and stabilises the free to move frame of the bike in such a way that the reference ride (Roadsurface or the real-time bike ride) behaviour is reflected in the control response. For the rest of the thesis, the roadsurface loadcase, which will be the reference simulation, will be referred to as *RS* and the Controlled Frame loadcase will be referred to as the *CF*.

2.2 Validation of SAA

The aim of SAA is to mimic the internal loads and stresses which are developed in the various components of the bike when it is ridden. This also forms the basis for the validation approach. SAA can be considered successful only when the loads developed at any arbritary point of the bike at any given time of the simulation matches the actual load measured at the corresponding time instance in the real-time measurement data. Since the RS Bike is our reference simulation, this means we need the loads at any given point on the CF Bike and the RS Bike to be the same. To that end, three so called *validation points* are selected. The point A is at the intersection of the rear frame and one of the dampers, point B is at the intersection of the front frame and the fork, and point C is at the intersection of the rear frame and the front frame. A brief overview of the validation process is illustrated in Figure 2.2.

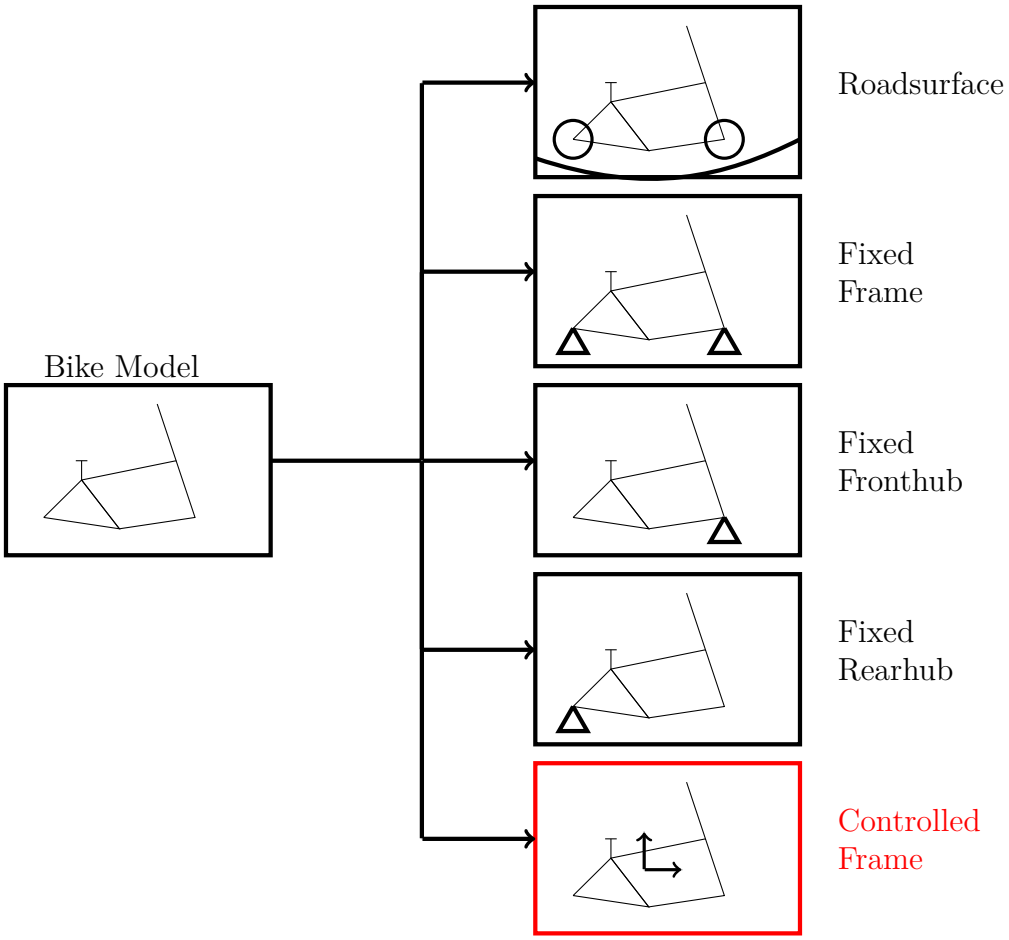

Figure 2.1: Various Loadcases in SAA

Error during Validation

During validation of SAA, it is necessary to objectify the errors between the CF and RS loadcases at the prescribed validation points. While plots directly comparing the forces developed at individual points in CF and RS may be helpful, in some cases the obtained improvement/degradation of results is not high enough to be refelected clearly from the plots. Thus, along with plots, tabulation of errors between the forces is also used. The parameters used for objectifying the errors are:

1. Mean percentage error $= \frac{1}{n}\sum_{i=1}^{n}\frac{|C_i - R_i|}{|R_i|} \cdot 100$, where n are the total number of data-points in the time series, C_i is the generalized force value at the i^{th} time-instant in the CF Simulation, and R_i is the generalized force value at the i^{th} time-instant in the RS Simulation.
2. RMSE $= \sqrt{\frac{1}{n}\sum_{i=1}^{n}(C_i - R_i)^2}$
3. R_2 (Coefficient of Determination), which is the measure of how similar in shape the force curves from CF and RS are.

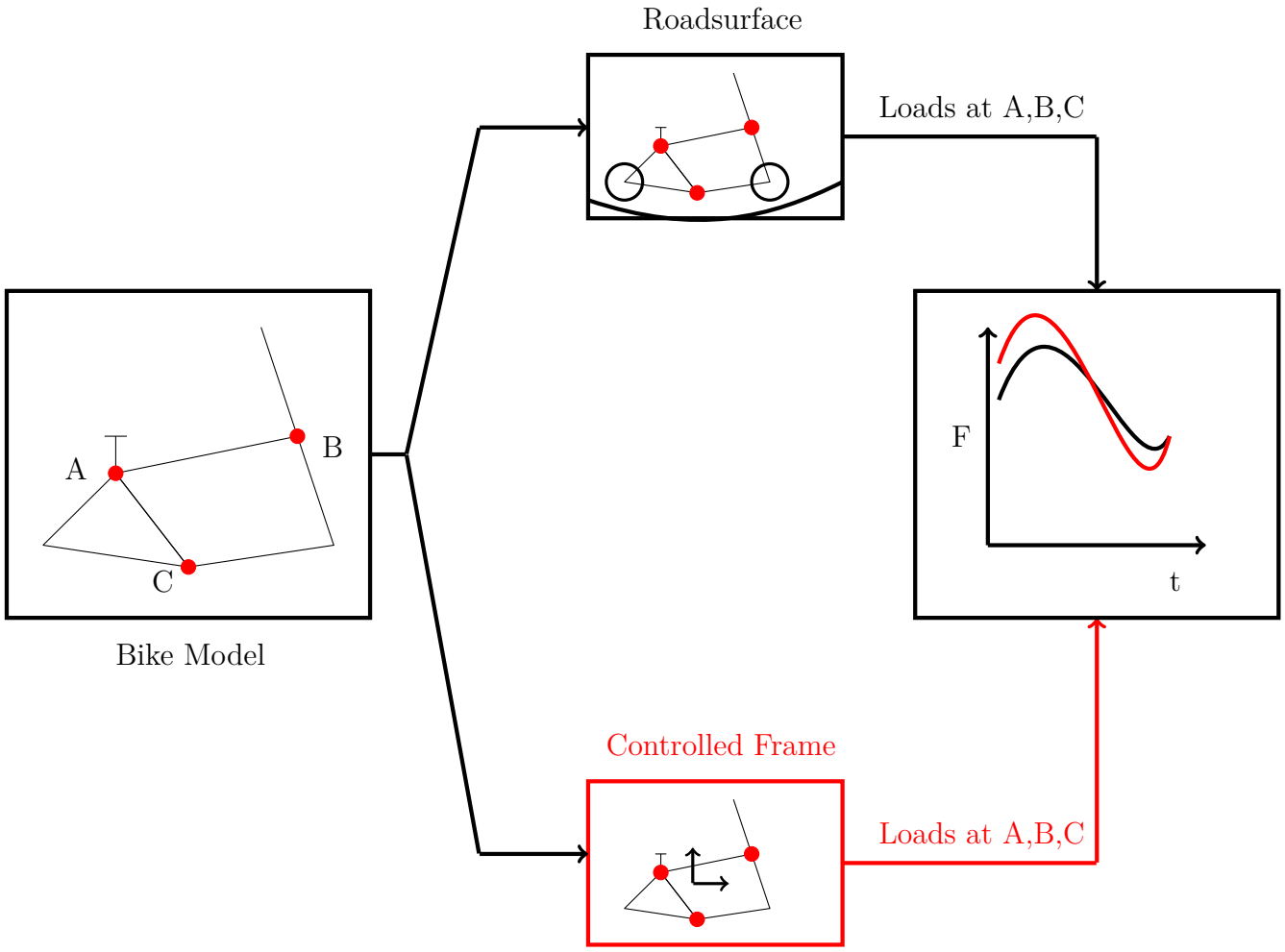

Figure 2.2: Validation of SAA

2.3 Loads workflow

The flow of loads calculation is illustrated in Figure 2.3. The simulation loads from RS are used to excite the bike in CF. When the real-time mesurement of loads are available, the simulation loads would be replaced by the measured loads. The simulation loads are the forces experienced at the *front hub, rear hub, pedals* and the *handlebar*. The idea is that these loads capture all the relevant information about the terrain and how the rider is riding the bike.

2.4 Control System setup

The control system simulation setup is illustrated in Figure 2.4. The setup utilizes the cosimulation functionalties provided by the SIMAT Block in Simulink, which allows multi-body simulations of the CF Bike to run in Simpack simultaneously alongside Simulink. Force elements specifically for transfering the controller forces/effort ($\mathbf{u}$) to the bike MBD model have been set up in Simpack. The controller is modelled in Simulink, since it provides extensive control system design functionalities. The SIMAT Block allows simultaneous data transfer between Simpack and Simulink during the Co-simulation, where

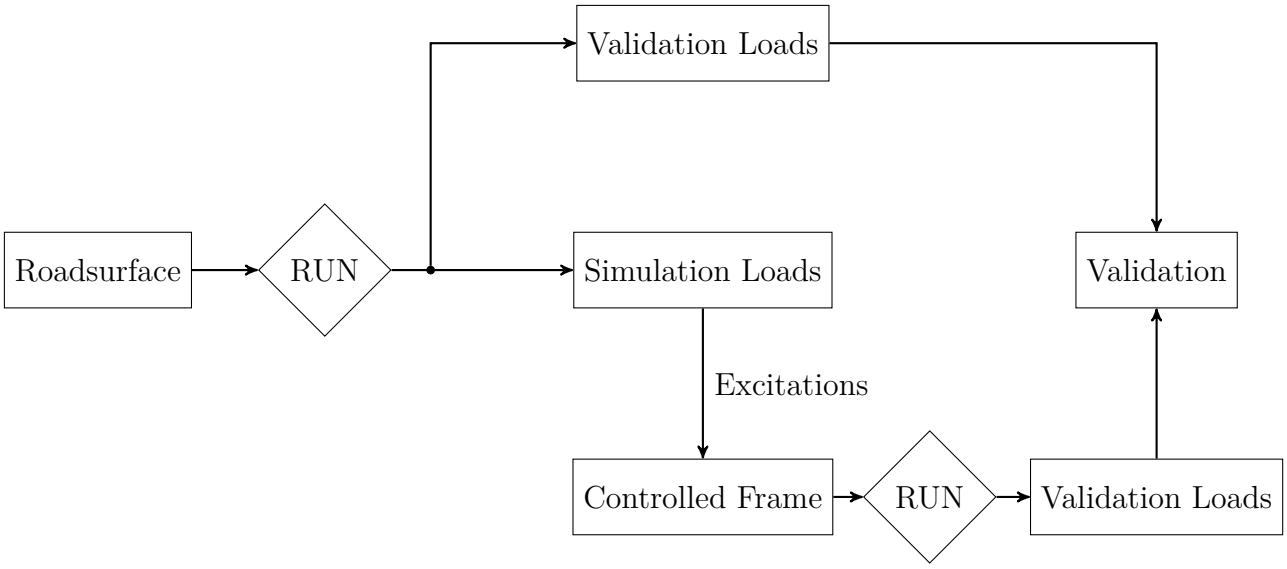

Figure 2.3: Loads Workflow

the controller effort is transferred from Simulink to Simpack, and the centre of gravity positions (translational and rotational) are transferred in the opposite direction.

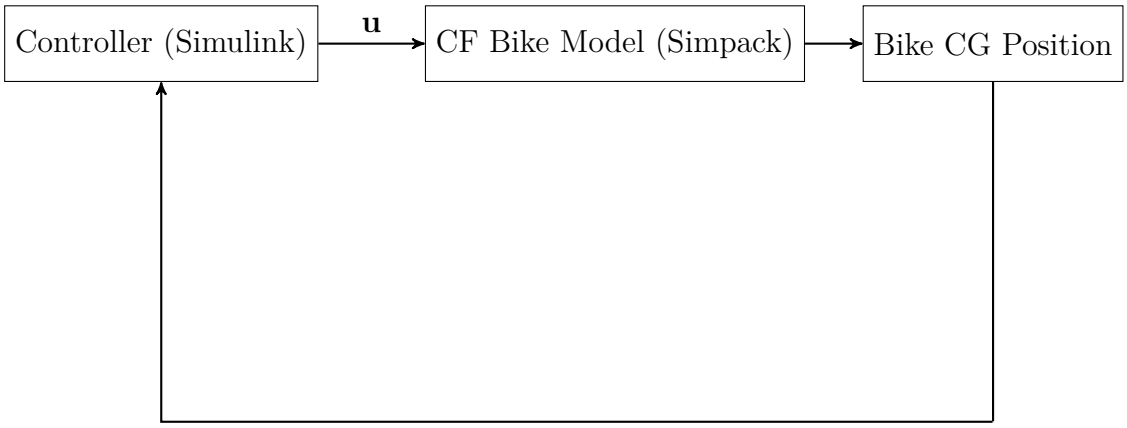

Figure 2.4: Control System Setup

Thus, a functional virtual control system is setup using both Simpack and Simulink. The controller effort from the controller consists of forces along the X and Y axes, and torque about the Z axis (axis coming out of the plane for the bike model in Simpack). The controller forces are applied at a singular point, the point being the centre of gravity of the bike.

It is important to note that a control system is necessary for the controlled frame loadcase, since in this loadcase the bike is free to move in 3D space and moreover is excited by external loads. In absence of any constraint on the bike frame, the frame would start to translate and rotate in an uncontrolled manner, thus showcasing a non-physical instability. The control system acts as a constraint, which prevents such instability in the bike frame.

3 Initial Controller Design

For the controller design, it is imperitive that a concrete control objective is set so that controller performance can be judged. The CF Bike is the plant for our control system and it is a MIMO (Multi-input, Multi-output) system. The inputs of our plant are the X-Y Planar forces and torque about Z axis, applied at the centre of gravity of the bike. The outputs are the translational positions of the bike and the rotation of the bike. Since each output would be coupled with other inputs (for example, the translation position of the bike would depend on the planar control forces and the control torque as well), our plant is quite interative. Irrespective of that, we use *Decentralized Control*, i.e. the MIMO system is treated as three independent SISO systems.

3.1 Control Objective

The control objective is derived from the aim of SAA: mimicing the behaviour of the actual bike ride (or the reference simulation ride) using control. Thus, our primary control performance parameters will be the closeness of CF and RS bike loads at the validation points mentioned in section 2.2. Thus, we are not necessarily very bothered about the traditional control system performance criteria like overshoot and other time domain peformance characteristics for regulation. Moreover, while using classical control methods, our tuning of the controller parameters can't include tradional tuning strategies like open/closed-loop shaping since reducing regulation/tracking error is not our goal. Thus, as the first iteration, imbalance compensation is attempted. Since the CF Bike experiences external excitations, there will be some net imbalance created, both translational and rotational, on the bike frame. The net rotational imbalance can be modelled as shown in Figure 3.1. It is important to note that the moment arm for each corresponding force will continuously change during the reference ride due to various inter-moving elements of the bike (for example, fork translates with respect to the front frame due to a spring connecting the two). For the control design in this thesis, which depends on a simulation reference, it is quite easy to extract the time variance of each moment arm, but when the loads are measured on the actual bike, recording the changing moving arms requires usage of additional sensors like IMUs which would record the position change of the different components of the bike. Keeping in mind economic feasibility and using minimal amount of sensors, this might be not the most suitable option. In such a scenario, an alternative is to measure the moment arms when the bike is static, and then assume that the change in the moment arms with time is negligible. The error in the actual imbalance on the bike and the imbalance estimated would then depend on various factors like the terrain and the manner of riding the bike, which would naturally affect the change of moment arms.

3.2 Pure Feedforward for Imbalance Compensation

A decentralized feedforward controller is used to feed in the negative of the imbalances estimated as shown in Figure 3.2. The idea is to compensate whatever net imbalance is created from the excitations provided to the CF Bike.

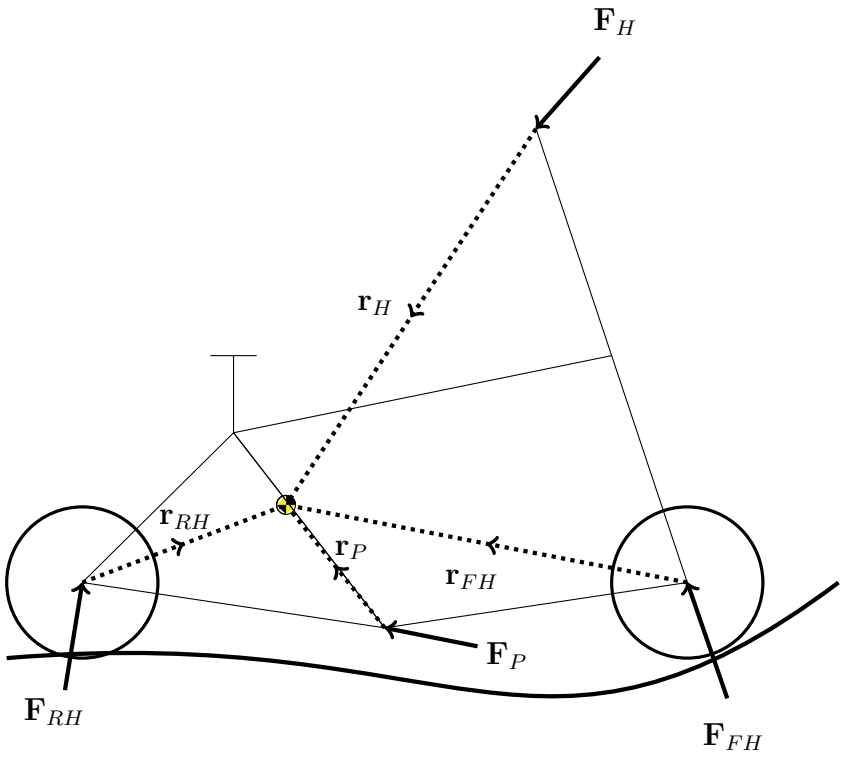

Figure 3.1: Net Imbalance force and torque on CF Bike

It is quite clear from Figure 3.3, which compares the loads from CF and RS bikes at point B, that such an approach is infact quite unsuitable. The bike frame becomes completely unstable in 3D space as a result of which its rotation degree of freedom explodes and hence the RS Bike forces are reflected very poorly. One plausible explanation for this would be the application method of the feedforward control forces on the CF Bike, which are localised only on the center of gravity of the bike. On the contrary, the excitations from the RS Bike are fed to the CF Bike at different discrete points with a given eccentricity from the center of gravity. In such a load application configuration, it might be possible that the expected compensation is not happening properly and the feedforward control forces are acting as additional excitations to the unconstrained CF Bike, hence inducing its uncontrollable and unstable movement in 3D space. Thus, we can conclude that a basic position control using feedback may be necessary in order to maintain the stability of the CF Bike in 3D space.

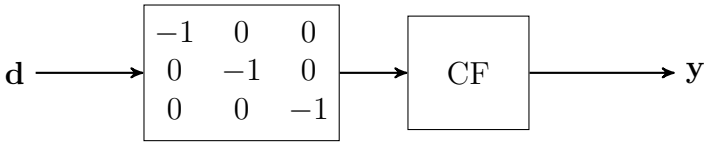

Figure 3.2: Pure feedforward Control

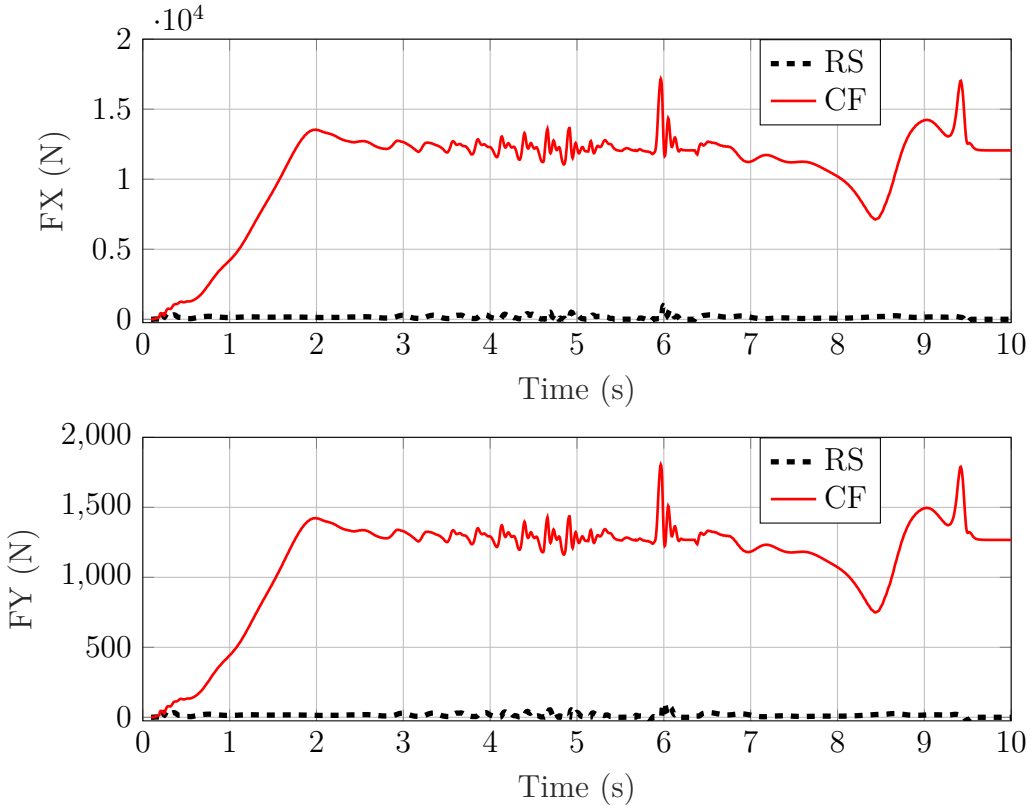

Figure 3.3: Loads at point B of CF under pure feedforward control

3.3 Classical Feedback Control

Figure 3.4 shows a decentralized feedback controller which generates the controller effort based on the output of the plant; the translational and angular position coordinates of the CF Bike. It is important to note that a positive feedback is used due to certain constraints in Simpack, and for now regulation is attempted, i.e. the reference position is zero.

PD Control

The feedback controller is set such that:

$$K_x = K_y = K_z = 100 + 500s$$

The tuning of the controller is done such that the derivative control is sufficiently high so as to increase the response speed and to counter imbalances with higher rates of change. The validation results can be visualized in Figures 3.5 to 3.7, while the errors between CF and RS has been quantified in Tables 3.1 to 3.3.

Thus, PD Control is promising for forces at point B and X component of forces at point A and C, while it shows mediocre performance for Y components of forces at A and C.

PID Control

Next, a PID Controller is tried with small integral action and the same proportional and derivative quantities. This controller doesn't lead to very significant modifications in the

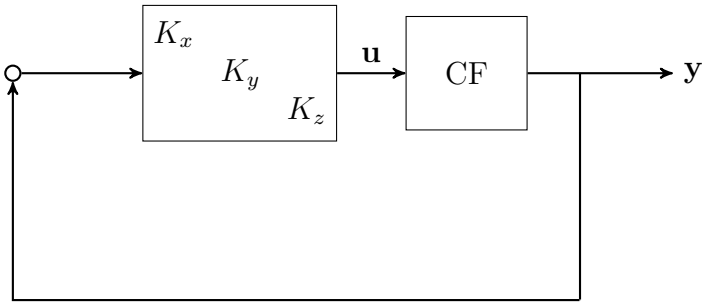

Figure 3.4: Classical Feedback Control

Forces	Mean Error (%)	RMSE	R_2
FX	3	127	0.98
FY	99	906	0

Table 3.1: Error Tabulation of Loads at Point A of CF under PD Feedback Control

Forces	Mean Error (%)	RMSE	R_2
FX	3	15	0.99
FY	3	2	0.99

Table 3.2: Error Tabulation of Loads at Point B of CF under PD Feedback Control

Forces	Mean Error (%)	RMSE	R_2
FX	4	149	0.95
FY	56	901	0.05

Table 3.3: Error Tabulation of Loads at Point C of CF under PD Feedback Control

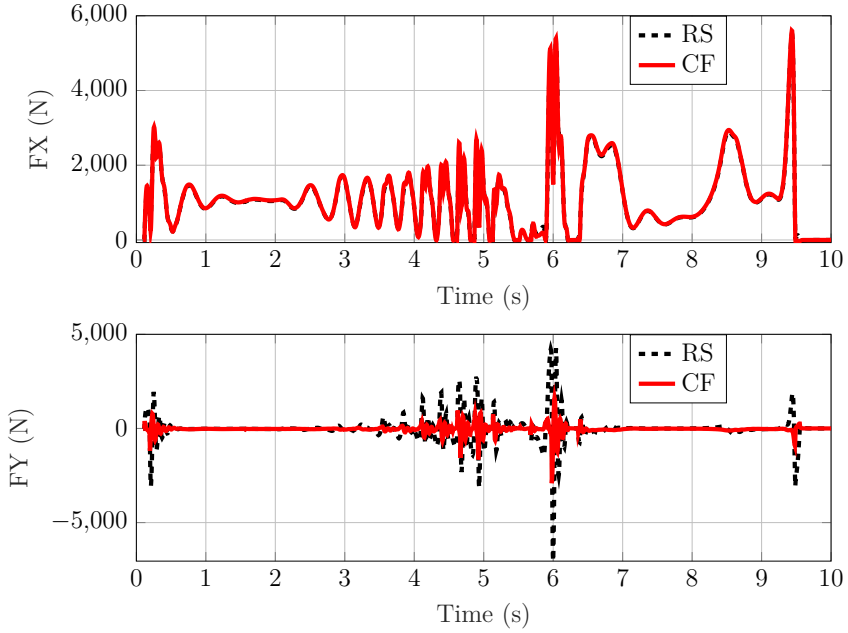

Figure 3.5: Loads at point A of CF under PD Feedback Control

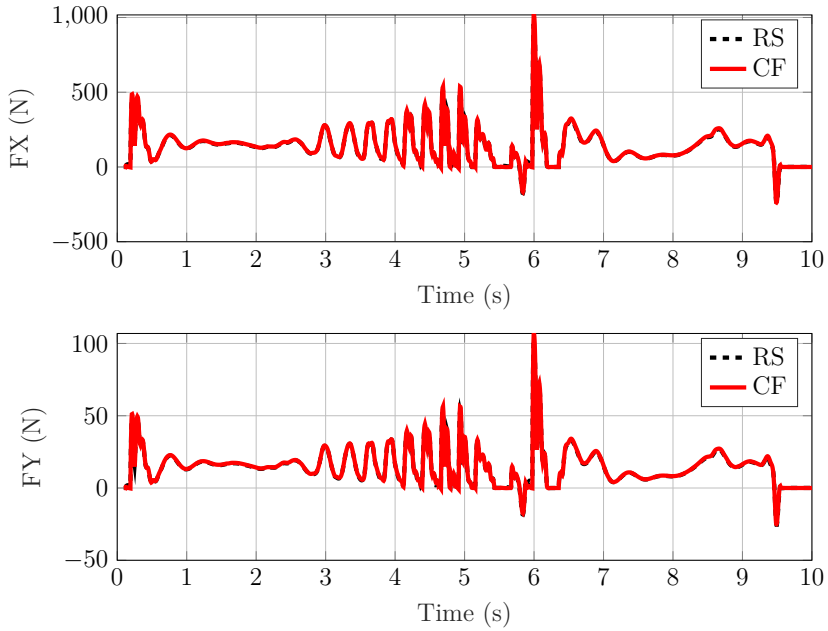

Figure 3.6: Loads at point B of CF under PD Feedback Control

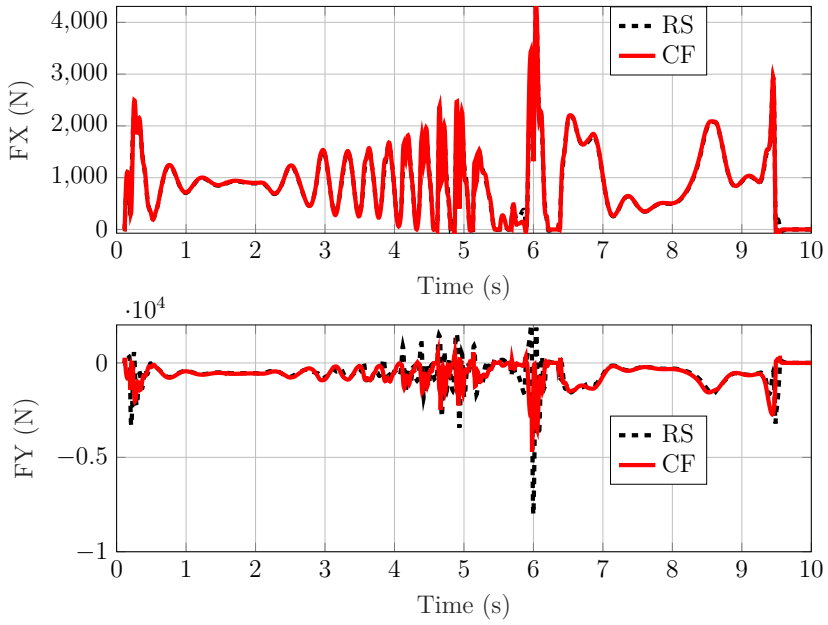

Figure 3.7: Loads at point C of CF under PD Feedback Control

performance of the PD Controller, which might be expected since the integral action activates on the basis of accumulation of error and for a small intergral gain value, the contribution from the integral action has quite a small effect. To observe some sort of changes in the performance, so as to get a better idea of whether the integral action is at all helpful, the PID Controller for the angular position of the bike is modified to:

$$K_z = 10 + 100s + \frac{1000}{s}$$

It is quite clear from Tables 3.4 to 3.6 that the Y force components correlation at A

Forces	Mean Error (%)	RMSE	R_2
FX	2	114	0.99
FY	56	488	0.5

Table 3.4: Error Tabulation of Loads at Point A of CF under PID Feedback Control with modified Z-Feedback

Forces	Mean Error (%)	RMSE	R_2
FX	3	14	0.99
FY	3	2	0.99

Table 3.5: Error Tabulation of Loads at Point B of CF under PID Feedback Control with modified Z-Feedback

Forces	Mean Error (%)	RMSE	R_2
FX	3	101	0.98
FY	35	516	0.52

Table 3.6: Error Tabulation of Loads at Point C of CF under PID Feedback Control with modified Z-Feedback

and C improves by quite a lot, while the X force components and the forces at B have not very large changes.

The correlation between the control effort and the imbalances estimated might help in understanding the control requirements. It can be seen in Figure 3.8 that the control effort in X and Y resemble the corresponding imbalances quite a lot. Thus, it seems like

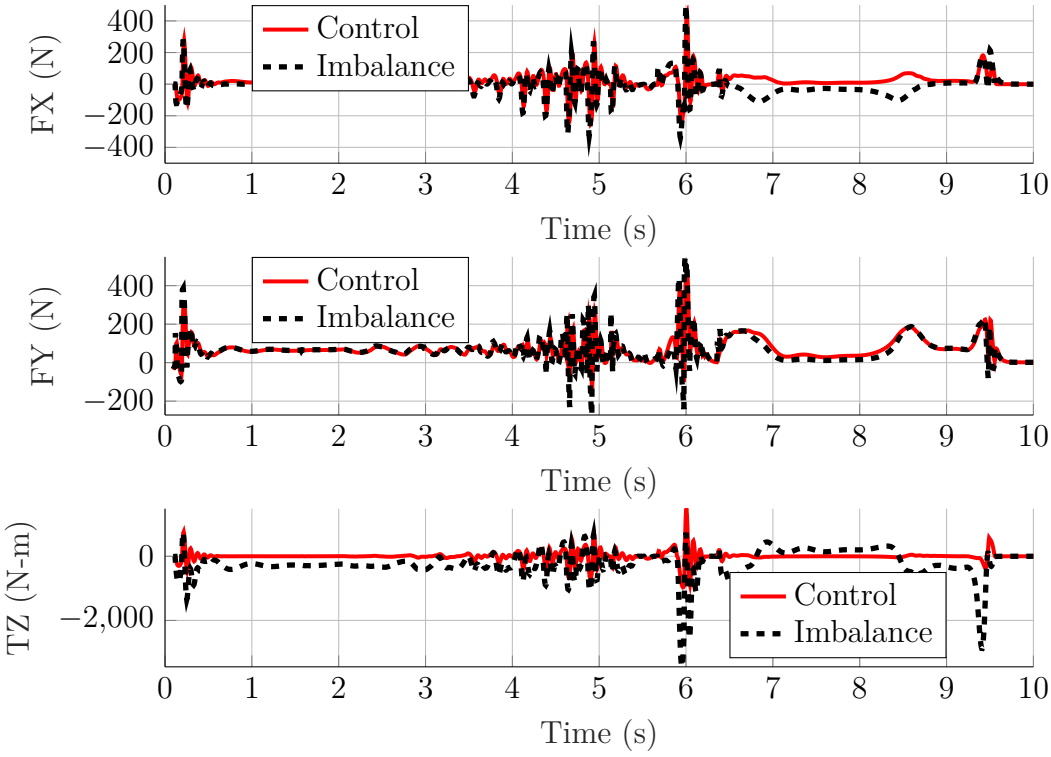

Figure 3.8: Comparison of Controller Effort and Net Imbalance on CF

the control forces as a result of position control try to recreate the imbalance forces experienced by the bike. It is observed after quite a lot of simulations with different controller parameters that better the correlation between the control forces and the imbalance forces is, better are the loads comparison between CF and RS at the validation points. It is also important to note that it was observed that for all classical PID and PD feedback cases, the control torque was always significantly less than the net imbalance torque experienced by the bike, as seen in Figure 3.8.

4 Limitations of SAA

Since the basic principle behind SAA is to reduce simulation effort by neglecting the rider and the terrain modelling, it has bound to have some limitations. This chapter focuses on the two main plausible limitations of SAA: *Neglected Bike Inertia* and *Noisy Measurements*.

4.1 Neglected Bike Inertia

In the current framework of the simulation setup for SAA, an attempt is made to keep the bike stabilized or fixed in space. In loadcases *Fixed Frame*, *Fixed Fronthub* and *Fixed Rearhub*, some component of the bike is always constrained, thus eliminating any movement which the bike will have during the actual ride. Similarly, in the regulation control system design for the CF bike, the position of bike center of gravity is controlled with respect to a zero reference point. Thus, by limiting the movement of the bike, we are effectively neglecting the inertia of the bike in the real-time ride. The inertia of the rider is already accounted for from the measured loads on the bike. Thus, the neglected bike inertia may be a plausible source of error for the SAA and may help explain the relatively poor validation of loads at points A and C as seen in Chapter 3. In the case that the bike inertia is found to be significant, the control objective can be modified to be a tracking problem, where the CF Bike follows the trajectory followed exactly by the RS Bike [BBJ21; JBB20]. When real-time measurements are used, that would naturally mean additional sensors in order to capture the movement of the bike.

All the simulations seen in Chapter 3 were for a rider of 90 Kg, and for a mountain bike, which is often quite light, the bike inertia is pretty negligable compared to the rider inertia. But as the weight of the rider decreases, the contribution of the bike inertia to the total inertia increases, and thus it is prudent to evaluate the performance of SAA for a so-called *worst-case scenario*, where the rider weight is assumed to be 45 kg, which can be attributed to the case when the rider is probably a child/teenager. Figure 4.1 shows the contribution of the bike inertia to the total inertia, and its comparison with the rider inertia for a 45 Kg rider. The total mass of the bike frame is taken to be 6.707 kgs, according to the bike which is modelled in Simpack.

It can be seen that the bike inertia, even for the worst case is quite small compared to the rider inertia, with the contribution of bike inertia being 12.97 %. It should be noted that only the translational inertia is analysed here, since comparing the rotary inertia of the rider and the bike is quite difficult as we do not have an idea about how the rider rides the bicycle and thus how would the mass distribution (mass moment of inertia) of the rider would change with time. Thus, for the following analysis, the inertia of any component of the bike is computed by the multiplication of the component mass by its translational acceleration.

In order to get a better insight into the contribution of the bike inertia, the inertia effects are added to the loads from the CF Bike at points A and C, which were the problem points for PD Control for 90 Kg rider. For point A, the inertia of the Damper is added to the force experienced by the damper from the rearframe, and for point C, the inertia of the rearframe is added to the force experienced by the rearframe from the

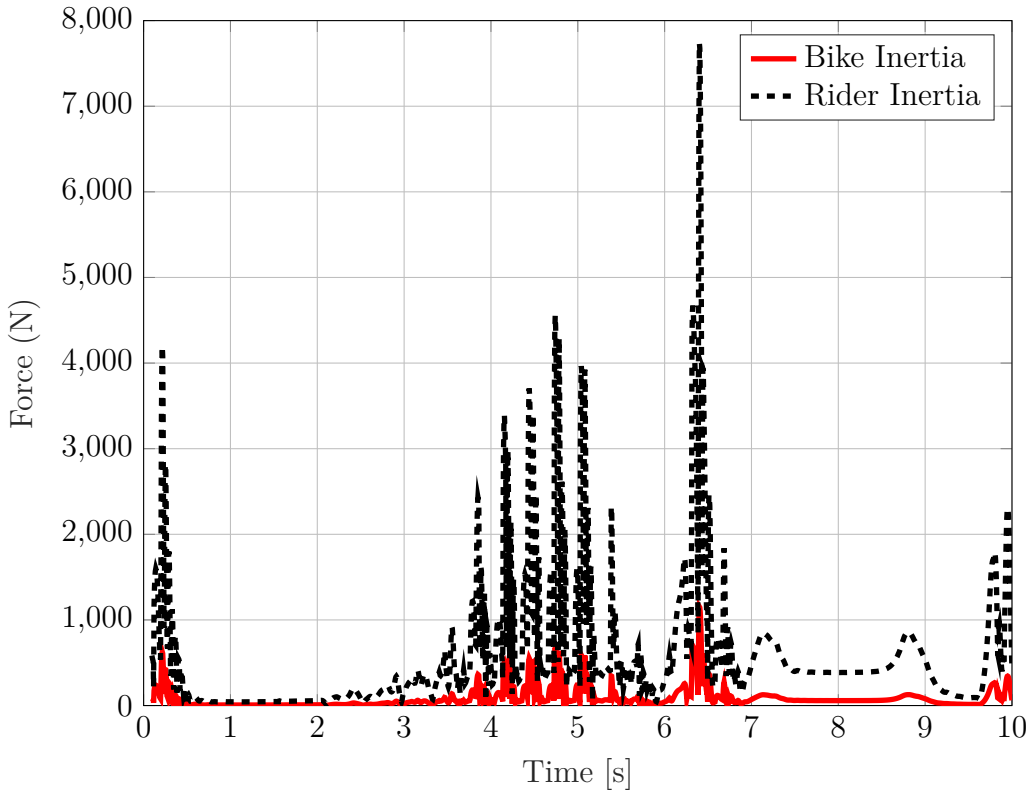

Figure 4.1: Contribution of Bike Inertia to the total inertia for a 45 Kg Rider.

frontframe. Figures 4.2 and 4.3 shows us that the added inertia effect has a negligible effect on the loads experienced at those particular points of the CF Bike. Thus, it would be prudent to conclude that the bike inertia doesn't pose a major limitation, even in the worst-case scenario. In order to verify the conclusion, the CF Bike is excited by the loads coming from a 45 Kg rider on the RS Bike and PD Control is used.

Classical PD Feedback Control for the worst-case

The validation loads errors are tabulated in Tables 4.1 to 4.3, and it can be observed that even though the errors increase, the magnitude of change is extremely small.

Forces	Mean Error (%)	RMSE	R_2
FX	8	135	0.95
FY	99	868	0.01

Table 4.1: Load Errors at Point A of CF with PD Control and 45 Kg rider

Forces	Mean Error (%)	RMSE	R_2
FX	7	15	0.96
FY	7	2	0.96

Table 4.2: Load Errors at Point B of CF with PD Control and 45 Kg rider

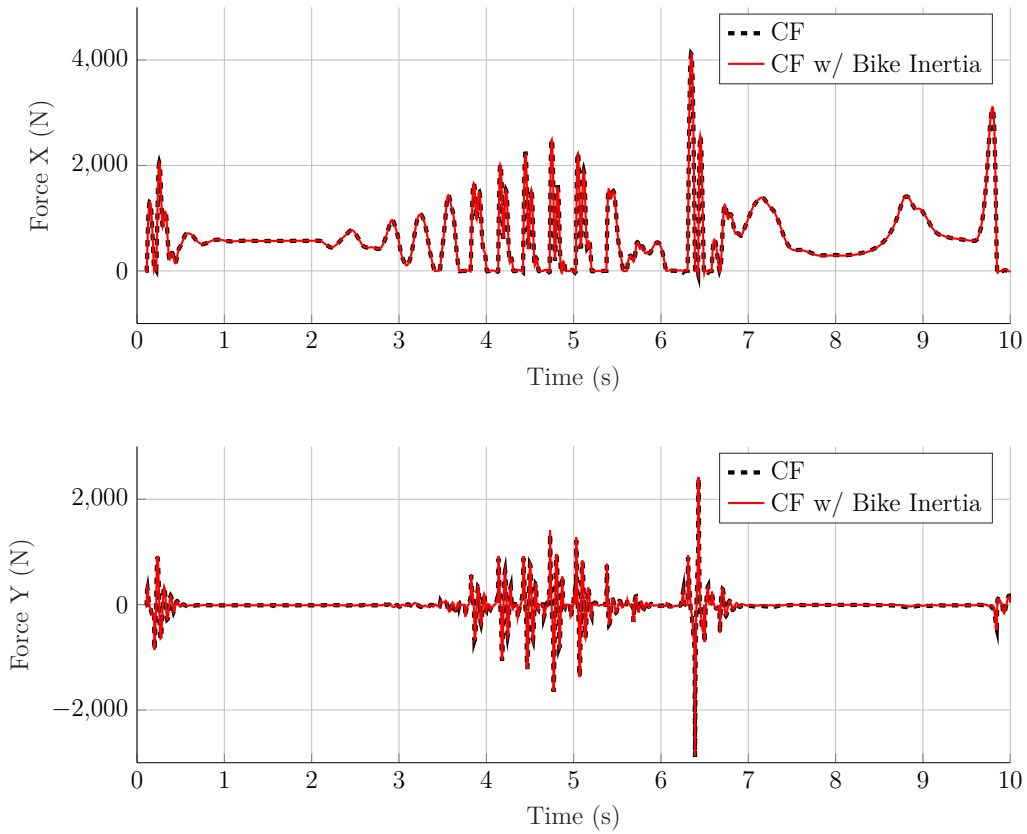

Figure 4.2: Added inertia effect to the force experienced by Damper from Rear-frame.

Forces	Mean Error (%)	RMSE	R_2
FX	11	159	0.87
FY	90	862	0

Table 4.3: Load Errors at Point C of CF with PD Control and 45 Kg rider

Thus, it can be concluded that the regulation of the CF Bike is enough as a control objective, as the bike inertia is always quite small compared to the rider inertia, and thus neglecting the bike inertia is quite a prudent strategy.

4.2 Measurment Noises

For all the results in this thesis, the reference data comes from the simulation of the RS Bike, which is quite convenient since we don't have to depend on sensors for measurement of loads. But when real-time sensing of loads is carried out on a real bike, the SAA will need to perform after being excited by the sensor-measured loads. In such a scenario, there will be some measurement noise that is involved in the measured loads. Other sources of noise, like riding on an extremely rough terrain and bad weather conditions can also exist. Thus, SAA should be robust to all these sources of noise. In order to see the effect of a noisy excitation on the current PD Control algorithm of the CF Bike, an artificial noise is generated in the loads from the RS Bike using a random number generator. The

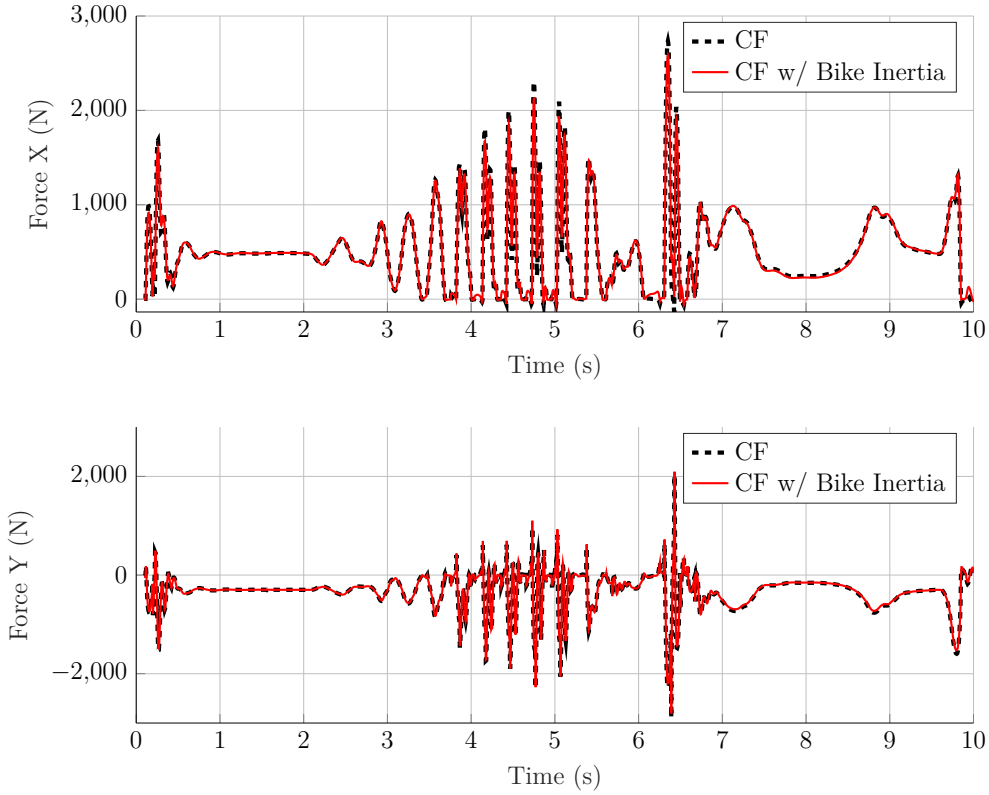

Figure 4.3: Added inertia effect to the force experienced by Rear-frame from Front-frame.

generated noise produces an uncertainty of less than to 100 % in the excitation value at each time step. Figure 4.4 compares the actual excitations and the noisy excitations.

PD Controller performance with Measurement Noise

The loads comparison at point B is shown in Figure 4.5, which was the most promising point for the PD Controller. It can be seen that the effect of the noise is transmitted directly to the performance of the controller, which decreases and can be seen from Tables 4.4 to 4.6 Thus, in order to attenuate the effect of the noise, filtering of the measured loads is attempted.

Forces	Mean Error (%)	RMSE	R_2
FX	45	746	0.63
FY	134	1527	0

Table 4.4: Load Errors at Point A of CF with PD Control and Measurment Noise

Low-pass filtering of measured loads

A *fourth-order low-pass butterworth filter* is used to filter out the high-frequency noise from the measured loads. A two-way filteration (forward followed by backward) filtering

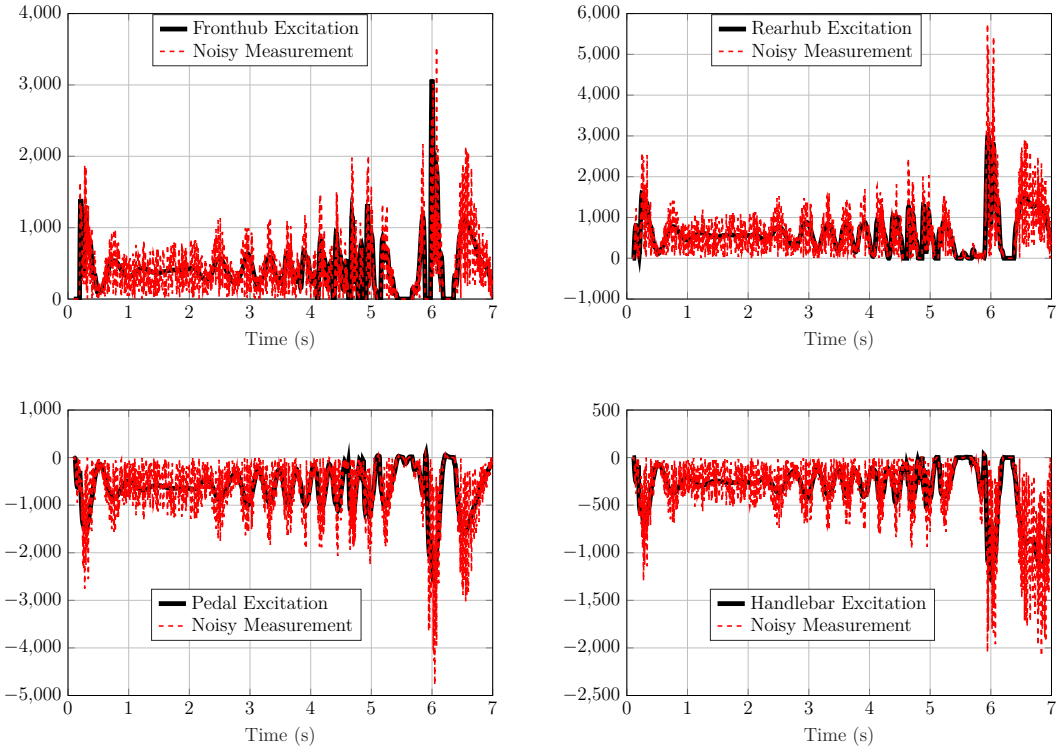

Figure 4.4: Noisy Measured Loads with random uncertainties

Forces	Mean Error (%)	RMSE	R_2
FX	46	97	0.62
FY	46	10	0.62

Table 4.5: Load Errors at Point B of CF with PD Control and Measurment Noise

Forces	Mean Error (%)	RMSE	R_2
FX	58	768	0.48
FY	111	1476	0.02

Table 4.6: Load Errors at Point C of CF with PD Control and Measurment Noise

is done in order to ensure that there is no phase shift between the noisy excitations and the filtered excitations. The modified loads workflow is illustrated in Figure 4.6.

The choice of the cut-off frequency is critical and should be suitable such that all the high frequency noise is eliminated, but at the same time the low-frequency information is not lost. For instance, for the sampling frequency of $200.1Hz$ of the excitations (2001 data-points in 10 seconds of simulation time of RS), three cut-off frequencies of $10Hz, 15Hz$ and $20Hz$ are tested, and it is found that for $10Hz$, the excitations get a little too smooth, thus implying a loss of low-frequency information, while for $20Hz$, there is still some noise left in the filtered loads. A nice balance is created by $15Hz$ cut-off and the filtered excitations are compared with the actual unaffected excitations from the RS Bike in Figure 4.7. The cut-off frequency will also be use-case dependent; a mountain bike riding through a mountain trail will require a higher cut-off freuquency than a city-bike

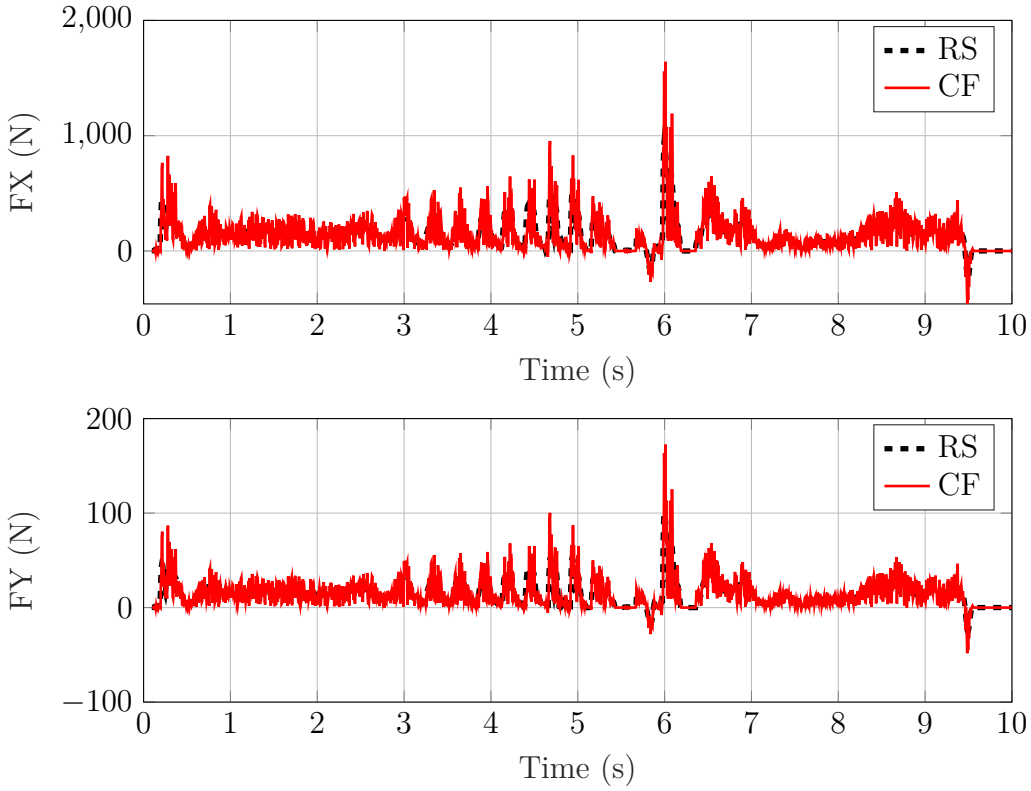

Figure 4.5: Loads at point B of CF with PD Control and Measurement Noise

riding through flat roads.

PD Controller Performance with filtered measured loads

As seen in Figure 4.8 and Tables 4.7 to 4.9, the validaion improves, but it's still not as good as when the excitations from RS had no noise. Thus, a the performance of SAA will also be determined by how good and prudent the filteration policy is.

Forces	Mean Error (%)	RMSE	R_2
FX	19	340	0.88
FY	103	899	0

Table 4.7: Load Errors at Point A of CF with PD Control and Measurment Noise filtered at 15 Hz Cut-off Frequency

Forces	Mean Error (%)	RMSE	R_2
FX	17	41	0.88
FY	17	4	0.88

Table 4.8: Load Errors at Point B of CF with PD Control and Measurment Noise filtered at 15 Hz Cut-off Frequency

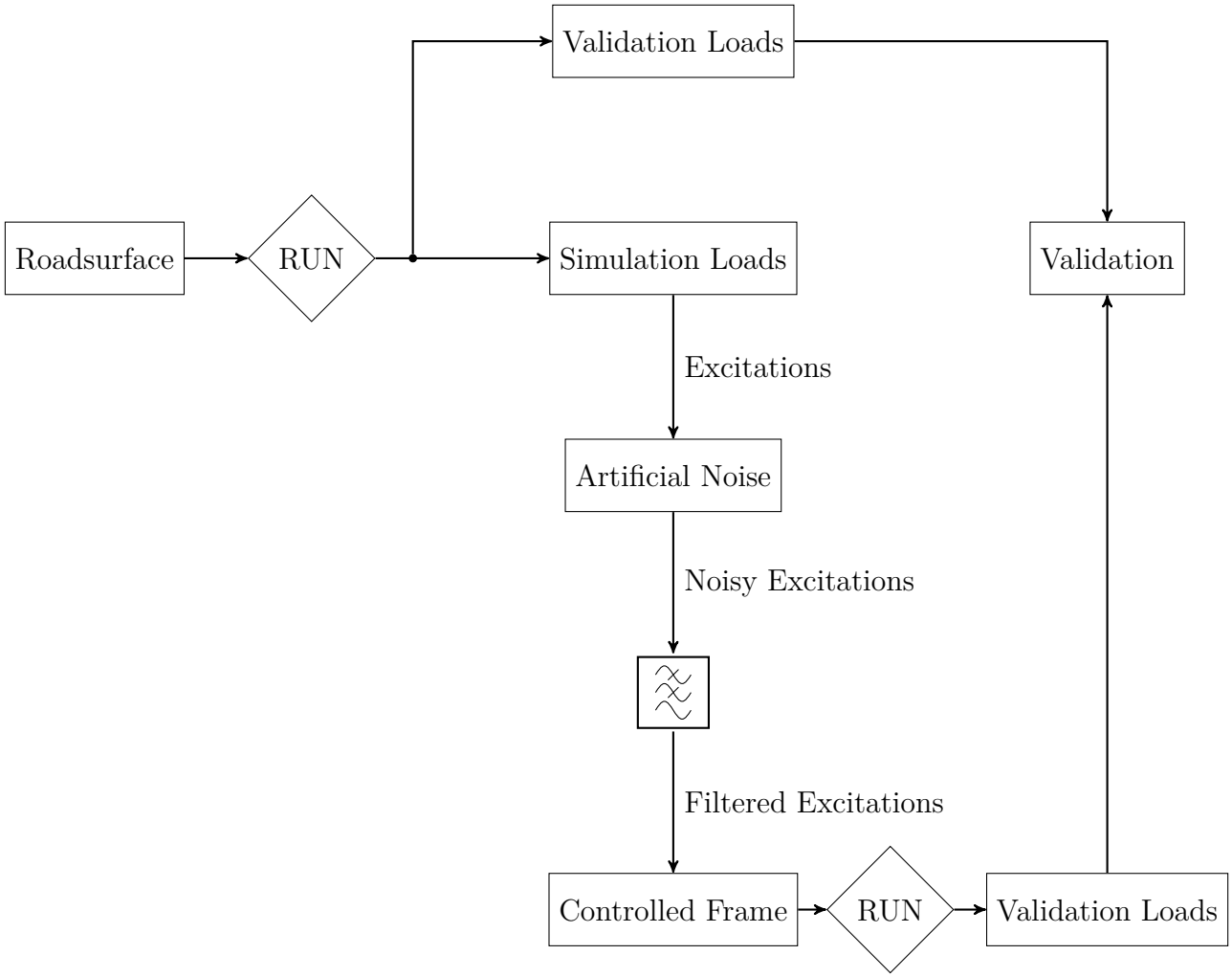

Figure 4.6: Loads workflow with noise and filtering

Forces	Mean Error (%)	RMSE	R_2
FX	25	364	0.79
FY	61	877	0.06

Table 4.9: Load Errors at Point C of CF with PD Control and Measurment Noise filtered at 15 Hz Cut-off Frequency

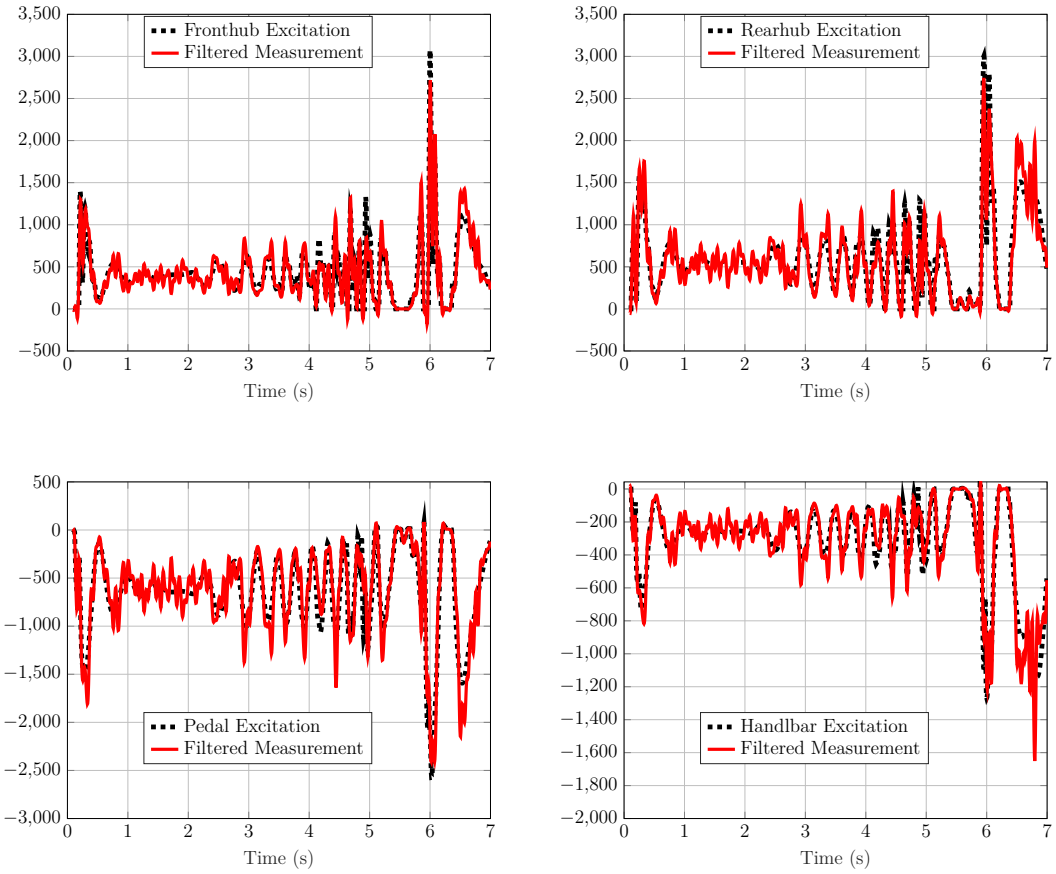

Figure 4.7: Noisy Measured Loads passed through a Low-Pass Butterworth Filter (15 Hz Cut-off)

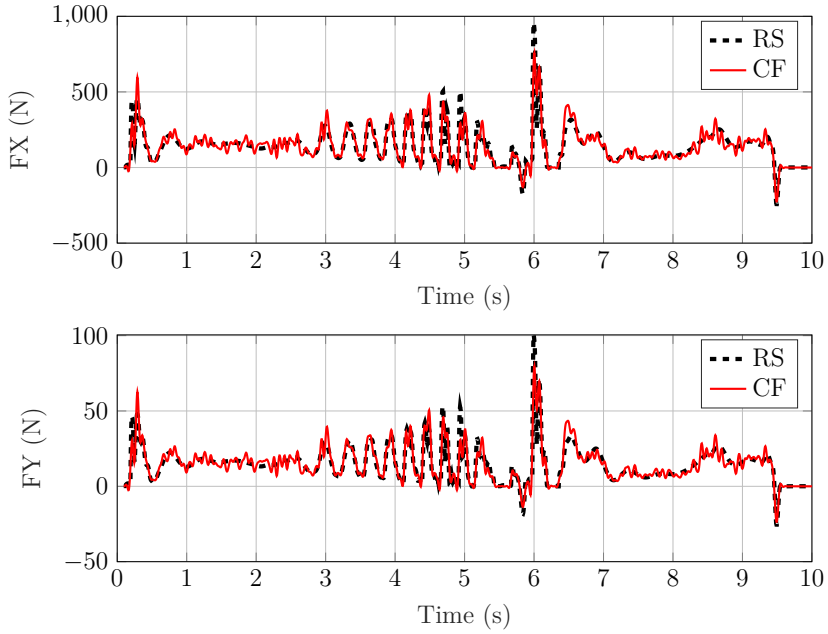

Figure 4.8: Loads at point B of CF with PD Control and Measurement Noise filtered at 15 Hz Cut-off Frequency

5 Feedback with Feedforward Control (Pre-control)

For pre-control, the net imbalance forces and torques are fed forward to the controller along with the feedback position control. The control system is illustrated in Figure 5.1. Thus, the controller effort **u** is a function of both the deviation of the bike centre of gravity from the reference position, and the net imbalances on the bike (**d**).

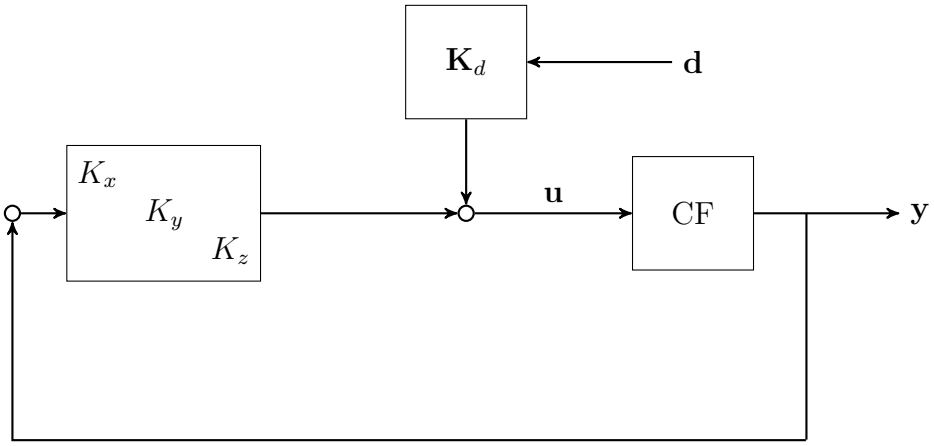

Figure 5.1: Pre-Control

5.1 Motivation

The idea behind the use of pre-control is the anticipation of the imbalance in the excitations which are fed to the CF Bike. The concept of imbalance anticipation is illustrated in Figure 5.2, where a set of hypothetical load plots for the handlebar and the rearhub for a small time frame Δt is shown. In the CF Bike simulation, the bike will start its deviation from its position primarily because of the imbalance, specifically when the imbalance is large enough to translate/rotate the bike frame. Then based on the resultant deviation, the position control will react and try to regulate the bike. This reaction will not coincide with the time instant at which the imbalance first starts, since the imbalance will take some time to be large enough to create the position change of the bike. Such a point where the position control starts reacting is depicted as B and t_B in the figure. When precontrol is used, we are directly feeding in the information about the imbalance to the controller, thus the controller will know the exact time at which the imbalance starts. The starting point of the imbalance is shown as A and t_A in the figure. Thus, the controller will start reacting faster to compensate the imbalance and ideally it should lead to a better control performance of the CF Bike.

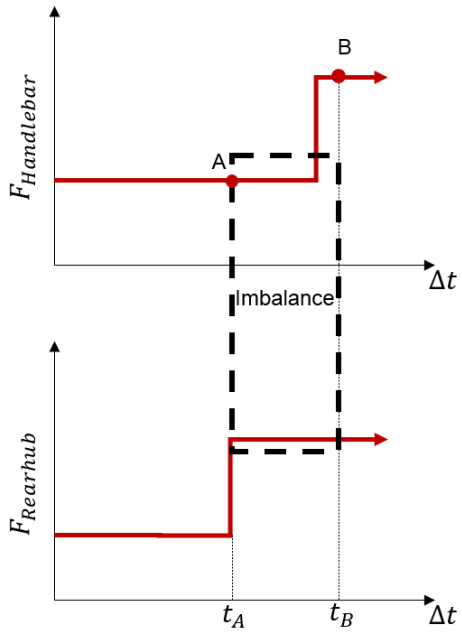

Figure 5.2: Imbalance anticipation

5.2 Varying Pre-Control Gains

The feedforward controller ($\mathbf{K}_d$) is considered to be decentralised like the feedback controller, and is considered to be constant.

$$\mathbf{K}_d = \begin{bmatrix} k_1 & 0 & 0 \\ 0 & k_2 & 0 \\ 0 & 0 & k_3 \end{bmatrix}$$

Thus, the controller effort looks like:

$$u_x = K_x \Delta x + k_1 d_x$$
$$u_y = K_y \Delta y + k_2 d_y$$
$$u_z = K_z \Delta \gamma + k_3 d_z$$

The tabulated controller performance for $k_1 = k_2 = k_3 = 1$ and $k_1 = k_2 = k_3 = -1$ and PD Feedback Control are shown in tables 5.1 to 5.6.

Forces	Mean Error (%)	RMSE	R_2
FX	3	128	0.98
FY	101	970	0.01

Table 5.1: Load Errors at Point A of CF with PD Control and Pre-control with gains $\{-1, -1, -1\}$

It can be seen that irrespective of the feedforward gains, the results don't improve or degrade by a very significant margin. Infact, it was observed after multiple simulation runs of different feedforward gains combined with different feedback controllers that using pre-control doesn't have a very (positive or negative) significant effect on the performance

Forces	Mean Error (%)	RMSE	R_2
FX	4	15	0.98
FY	4	2	0.98

Table 5.2: Load Errors at Point B of CF with PD Control and Pre-control with gains $\{-1, -1, -1\}$

Forces	Mean Error (%)	RMSE	R_2
FX	4	154	0.95
FY	59	972	0.05

Table 5.3: Load Errors at Point C of CF with PD Control and Pre-control with gains $\{-1, -1, -1\}$

Forces	Mean Error (%)	RMSE	R_2
FX	3	129	0.98
FY	103	914	0

Table 5.4: Load Errors at Point A of CF with PD Control and Pre-control with gains $\{1, 1, 1\}$

Forces	Mean Error (%)	RMSE	R_2
FX	4	16	0.98
FY	4	2	0.98

Table 5.5: Load Errors at Point B of CF with PD Control and Pre-control with gains $\{1, 1, 1\}$

Forces	Mean Error (%)	RMSE	R_2
FX	4	155	0.95
FY	59	912	0.03

Table 5.6: Load Errors at Point C of CF with PD Control and Pre-control with gains $\{1, 1, 1\}$

that pure feedback control was showing. Thus, our hypothesis regarding the perceived benefit of pre-control is more or less proved wrong.

5.3 Eliminating CF Angular Position Feedback

As mentioned in Chapter 3, for almost all purely feedback controllers, the control torque (u_z) was always significantly less than the net imbalance torque experienced by the bike. This is also true when pre-control is used. The likely reason for this might be the compensation in position provided by the feedback of the rotation of the CF Bike. Thus, the feedback of the angular position of the CF Bike (γ) is eliminated along with PD Control of the X and Y positions of CF Bike along with pre-control still activated. In this case, we have to be cautious since about the Z axis, a feedforward torque is directly fed without feedback, and as observed in section 3.2 of chapter 3, directly feedforwarding forces or torques without feedback leads to instability of the CF Bike. Thus, the pre-control gain

about the Z axis is kept very low. Tables 5.7 to 5.9 show the tabulated performance with no Z-feedback.

Forces	Mean Error (%)	RMSE	R_2
FX	15	324	0.95
FY	13	177	0.94

Table 5.7: Load Errors at point A of CF with no Z Feedback and Pre-control with gains $\{0, 0, -0.1\}$

Forces	Mean Error (%)	RMSE	R_2
FX	142	359	0.31
FY	142	38	0.31

Table 5.8: Load Errors at point B of CF with no Z Feedback and Pre-control with gains $\{0, 0, -0.1\}$

Forces	Mean Error (%)	RMSE	R_2
FX	12	192	0.96
FY	25	304	0.89

Table 5.9: Load Errors at point C of CF with no Z Feedback and Pre-control with gains $\{0, 0, -0.1\}$

It can be seen that the control performance drastically improves, especially for the Y component of the forces at points A and C but at the same time, it worsens significantly at point B for both X and Y components.

5.4 Unactuated Angular Movement of CF

Building on the idea introduced in section 5.3, the angular degree of freedom of the CF bike is left unmodified, i.e. there is no Z feedback and no Z pre-control. Figures 5.3 to 5.5, and tables 5.10 to 5.12 showcase extremely good controller performance as compared to all the controller parameters attempted.

Forces	Mean Error (%)	RMSE	R_2
FX	2	118	0.98
FY	1	30	1

Table 5.10: Load Errors at point A of CF with no Z Feedback and Pre-control

Forces	Mean Error (%)	RMSE	R_2
FX	2	15	0.98
FY	2	2	0.98

Table 5.11: Load Errors at point B of CF with no Z Feedback and Pre-control

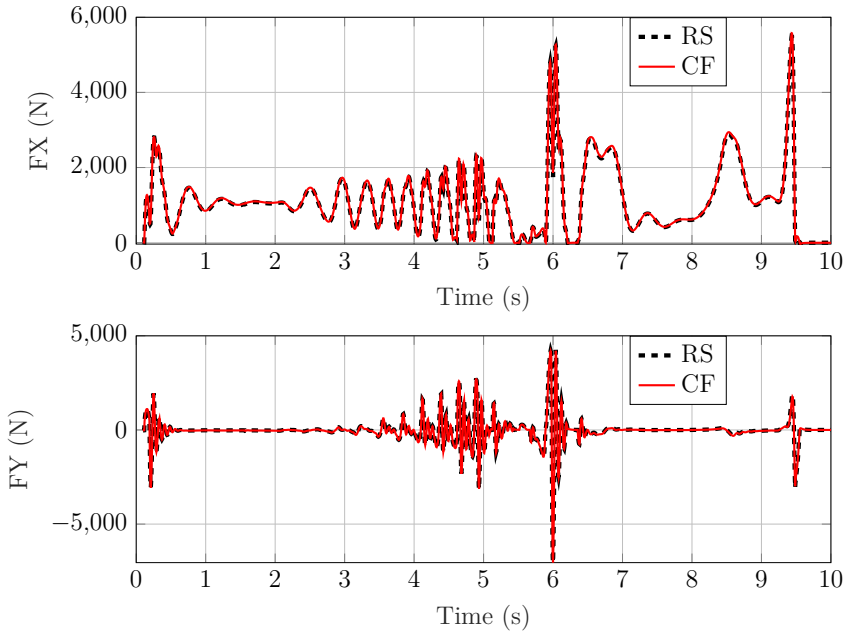

Figure 5.3: Loads at point A of CF with no Z Feedback and Pre-control

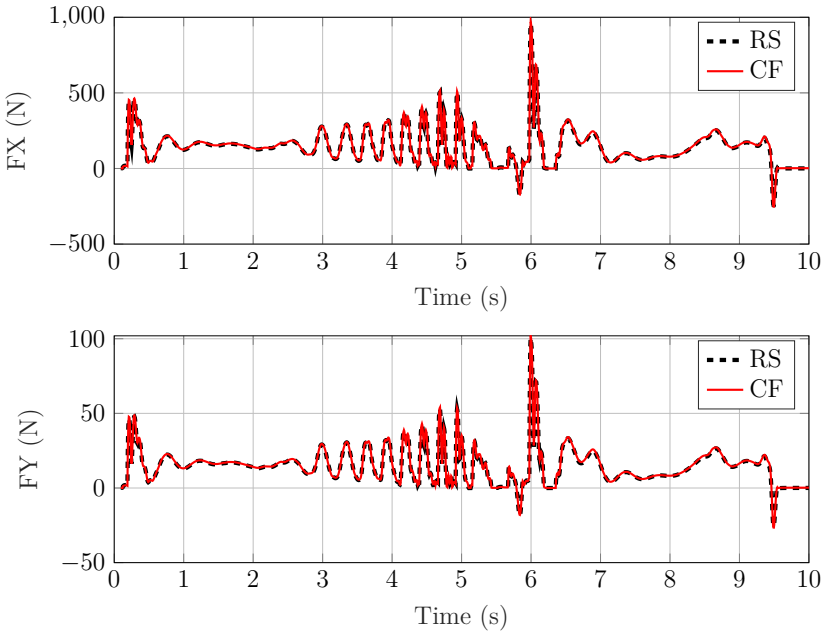

Figure 5.4: Loads at point B of CF with no Z Feedback and Pre-control

Forces	Mean Error (%)	RMSE	R_2
FX	1	89	0.98
FY	4	147	0.96

Table 5.12: Load Errors at point C of CF with no Z Feedback and Pre-control

Thus, it can be said that SAA works extremely well when a position control algorithm only for the translational degrees of freedom of the bike, while the rotational degreee of

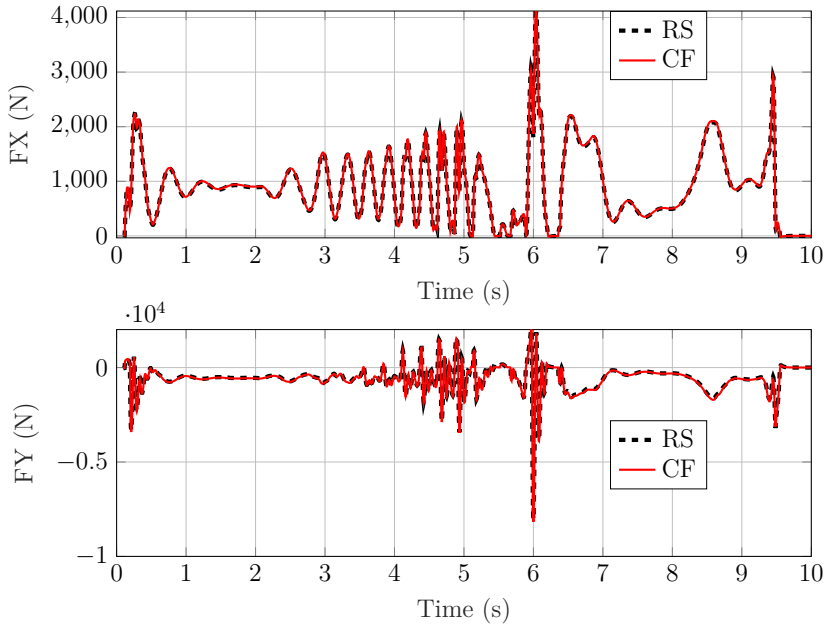

Figure 5.5: Loads at point C of CF with no Z Feedback and Pre-control

freedom is left unactuated. Additionally, while the idea of pre-control was promising, using it had no significant effect on the controller performance. The good functioning of the SAA with no rotational degree of freedom actuation was reflected by the PID Controller introduced in section 3.3 of chapter 3. There the integral action for the rotational degree of freedom dominated as compared to the derivative and proportional actions, and since the integral action produces actuation based on the accumulated error over time, the overall control torque produced was quite low as compared to the PD controller introduced a section before. Thus, for a low actuated rotational degree of the freedom, the PID Controller was showing quite good results.

The possible explanation for no Z-actuation showing such a good controller performance may be attributed to that fact that in the reference simulation, the RS Bike might have significant rotary inertia, which as mentioned in section 4.1 can't be explicitly compared with the rider rotary inertia in SAA. When the angular movement of the CF Bike is left completely unconstrained, the neglected rotary inertia might be getting compensated for, and thus leading to extremely good controller results. It should also be noted that when real-time measurement of loads are used, rotary inertia of the bike may play a very important role depending on the track on which the bike is ridden. Thus, it would be prudent to leave the angular movement of the CF Bike unactuated.

6 Future Scope and Summary

This chapter outlines the future scope and possible work packages which can be derived from the work covered in this thesis. There are three main ideas which can be pursued in order to improve SAA for the CF loadcase; *Feedforward Control for ideal disturbance rejection*, *Application of controller forces on multiple bike frame points* and *using an elastic bike frame*.

6.1 Ideal Disturbance Rejection

For the feedforward part introduced in the previous chapter, only constant gain values were used. While not in the scope of this thesis, it is interesting to explore the case when the feedforward gains are transfer functions. Figure 6.1 illustrates the control system designed for disturbance rejection. **d** is the vector of excitations fed to the CF bike, which in this context is taken as the disturbance signal. The feedback controller is decentralized

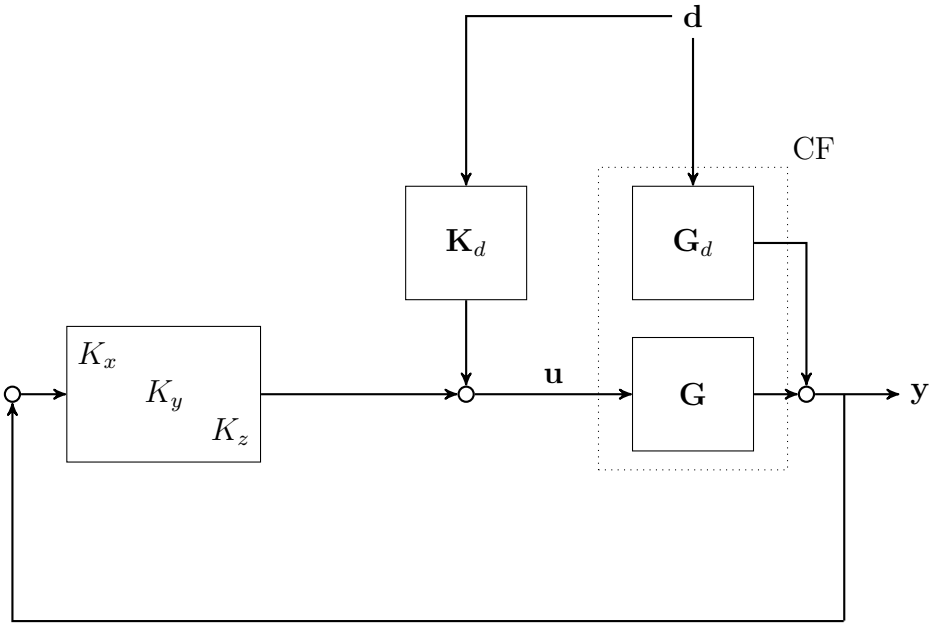

Figure 6.1: Ideal Disturbance Rejection

as before, and $\mathbf{K}_d$ is the feedforward transfer function matrix. It is important to note that for this control system design, the dynamic model of the CF Bike needs to be linearized. Once a linearized model is obtained, the plant transfer function matrix ($\mathbf{G}$) and the disturbance dynamics transfer function matrix ($\mathbf{G}_d$) can be obtained. Then, for ideal disturbance rejection, i.e. the output $\mathbf{y}$ doesn't get affected by $\mathbf{d}$, $\mathbf{K}_d$ can be derived as:

$$
\begin{aligned}
& \boldsymbol{y} = \boldsymbol{G}_d\boldsymbol{d} + \boldsymbol{G}\boldsymbol{u} \\
& \boldsymbol{u} = \boldsymbol{K}\boldsymbol{y} + \boldsymbol{K}_d\boldsymbol{d} \\
\implies & \boldsymbol{y} = \boldsymbol{G}_d\boldsymbol{d} + \boldsymbol{G}\boldsymbol{K}\boldsymbol{y} + \boldsymbol{G}\boldsymbol{K}_d\boldsymbol{d} \\
\implies & \boldsymbol{y} = (\boldsymbol{I} - \boldsymbol{G}\boldsymbol{K})^{-1}(\boldsymbol{G}_d + \boldsymbol{G}\boldsymbol{K}_d)\boldsymbol{d}
\end{aligned}
$$

For $\mathbf{K}_d = -\mathbf{G}^{-1}\mathbf{G}_d$, ideal disturbance rejection is achieved theoretically.

System Modelling

For obtaining the plant and disturbance dynamics, system modelling needs to be carried out of the CF Bike. To that end, a simplistic dynamic model of the CF Bike can be made, from which the equations of motion can be derived and the state-space matrices can be obtained. Alternatively, Simpack also has a functionality where it linearizes the model about an equilibrium point, and directly gives out the state-space matrices. In this section, a brief overview of the state-space modeling and the subsequent transfer function matrix calculation is given.

The outputs of the system are assumed to be the CF Bike CoG planar degrees of freedom (translations along X and Y, and rotation about Z), the system inputs are considered to be the controller/actuation effort on the CoG of the bike frame, and the excitations fed to the CF Bike at the 4 points (handlebar, pedal, front frame, rear frame). 10 states are recognised by Simpack for the state space modelling, effectively meaning 5 independent minimal degrees of freedom and their corresponding velocities. Then, the dynamics of the bike can be derived as:

$$\begin{aligned} \dot{\boldsymbol{x}} &= \boldsymbol{A}\boldsymbol{x} + \boldsymbol{B}\boldsymbol{u} \\ \boldsymbol{y} &= \boldsymbol{C}\boldsymbol{x} + \boldsymbol{D}\boldsymbol{u} \\ \boldsymbol{G}_{CF} &= \boldsymbol{C}(s\boldsymbol{I} - \boldsymbol{A})^{-1}\boldsymbol{B} + \boldsymbol{D} \end{aligned}$$

The transfer function matrix $\mathbf{G}_{CF}$ can be decomposed as,

$$\boldsymbol{G}_{CF} = \begin{bmatrix} \boldsymbol{G} & \boldsymbol{G}_d \end{bmatrix}$$

While such an approach looks extremely promising theorectically, there are few plausible bottlenecks which can appear while implementation. For instance, for perfect disturbance rejection, we need to invert the plant dynamics transfer function matrix $\mathbf{G}$ and depending on the transfer funcion matrix zeros, that might not be possible at every point. Additionally, the state-space matrices given out by Simpack are of a very high order which makes the simulation time extremely long and sometimes even leads to convergence issues. Thus, model reduction needs to be carried out on the model extracted from Simpack, or alternatively, a simplified dynamic model needs to be constructed of the CF Bike and the state-space matirces need to be computed manually from the subsequent equations of motion.

6.2 Modifying application of control forces

For the entirety of the work carried out in this thesis, the control forces were applied only at a singular point of the bike; the centre of gravity. Another interesting research direction would be exploring if there are better ways of feeding the controller forces to the bike frame by means of increasing the number of points at which the controller force is applied, or even making use of elements like RBE2/RBE3 in case flexible bodies are used to model the bike.

6.3 Modelling the bike using flexible bodies

To capture the real behaviour of the bike frame and its components better, elastic bodies may be used to model the bike. This kind of modelling would also be suitable for the CF bike loadcase, since there are no external constraints on the bike in this loadcase, and the standard external contrainsts can not be used with elastic bodies. Additionally, if elastic bodies are used, we would need to use standard FEM elements like RBE2 or RBE3 for the application of the control forces to the bike frame.

6.4 Summary

In this thesis, the *Controlled Frame* loadcase in SAA was studied in order to obtain the best performing controller, with the performance metrics being how well internal loads from a reference simulation are reflected in the SAA Bike model. Classical control methods are used, and the concept of pre-control using feedforward controllers is explored. It is concluded that while pre-control has no sigificant effect on pure feedback control, leaving the angular rotation of the bike model unconstrained and unactuated leads to be best controller performance.

Along with controller design, possible pitfalls of SAA are also explored, namely negligence of bike inertia and measurement noises. Based on inertia and noise analysis, it is found out that while bike translational inertia plays a negligible role in the total inertia, the controller performance would be significantly dependent on how well the noise from the sensors measuring the loads on a real bike are filtered out.

Bibliography

[BBJ21] Blanchette, C.; Boisvert, M.; Joubert, N.; Rancourt, D.; Desrochers, A.
Dynamic input loads evaluation of a recreational vehicle frame using multibody dynamics hybrid modeling validated with experimental and full analytical modeling data
In: Advances in Mechanical Engineering, 13 (2021) 8, DOI 10.1177/16878140211034608.

[Bru10] Brust, E.
Betriebsfestigkeit fertig montierter Fahrräder
In: Materials Testing, 52 (2010) 3, pp. 148–151.

[BS10] Blümel, M.; Senner, V.
Aktuelle Betriebslastenermittlung an Sportfahrrädern
In: Materials Testing, 52 (2010) 3, DOI 10.3139/120.110118, pp. 142–147.

[CAE16] Covill, D.; Allard P. adn Drouet, J.-M.; Emerson, N.
An Assessment of Bicycle Frame Behaviour under Various Load Conditions Using Numerical Simulations
In: Procedia Engineering, 147 (2016), DOI 10.1016/j.proeng.2016.06.269, pp. 665–670.

[DTC13] Doria, A.; Tognazzo, M.; Cusimano, G.; Bulsink, V.; Cooke, A.; Koopman, B.
Identification of the mechanical properties of bicycle tyres for modelling of bicycle dynamics
In: Vehicle System Dynamics, 51 (2013) 3, DOI 10.1080/00423114.2012.754048, pp. 405–420.

[FS07] Füglein, E.; Scheller, C.
Folgenschwere Fahrradunfälle durch unzureichende Prüfung?
In: Materials Testing, 49 (2007) 11, pp. 12–15.

[HHS11] Hölsel, C.; Hoechtl, F.; Senner, V.
Operational loads on sport bicycles for possible misuse
In: Procedia Engineering, 13 (2011), DOI 10.1016/j.proeng.2011.05.054, pp. 75–80.

[Jac17] *Mehr Sicherheit bei Pedelecs*
https://2017.lbf-jahresbericht.de/leistungen/projektuebersicht/zuverlaessigkeit/mehr-sicherheit-bei-pedelecs/ (visited on 04/27/2023).

[JBB20] Joubert, N.; Boisvert, M.; Blanchette, C.; St-Amant, Y.; Desrochers, A.; Rancourt, D.
Frame loads accuracy assessment of semianalytical multibody dynamic simulation methods of a recreational vehicle
In: Multibody system dynamics, 50 (2020) 2, DOI 10.1007/s11044-020-09756-8, pp. 189–209.

[KSM08] Kooijman, J. D. G.; Schwab, A. L.; Meijaard, J. P.
Experimental validation of a model of an uncontrolled bicycle
In: Multibody system dynamics, 19 (2008) 1-2, DOI 10.1007/s11044-007-9050-x., pp. 115–132.

[MPR07] Meijaard, J.; Papadopoulos, J. M.; Ruina, A.; Schwab, A.
Linearized dynamics equations for the balance and steer of a bicycle: a benchmark and review
In: Proceedings of The Royal Society A, 463 (2007) 2084, DOI 10.1098/rspa.2007.1857, pp. 1955–1982.

[MX14] Mei, Y. H.; Xie, Q. S.
Fatigue Loads Prediction Based on a Hybrid Road Approach
In: Advanced Materials Research (, 2014) 989-994, DOI 10.4028/www.scientific.net/AMR.989-994.3363, pp. 3363–3366.

[Red05] Redfield, R.
Large motion mountain biking dynamics
In: Vehicle System Dynamics, 43 (2005) 12, DOI 10.1080/00423110412331289844, pp. 845–865.

[RTV19] Risaliti, E.; Tamarozzi, T.; Vermaut, M.; Cornelis B.; Desmet, W.
Multibody model based estimation of multiple loads and strain field on a vehicle suspension system
In: Mechanical Systems and Signal Processing, 123 (2019), DOI 10.1016/j.ymssp.2018.12.024, pp. 1–25.

[SM13] Schwab, A. L.; Meijaard, J. P.
A review on bicycle dynamics and rider control
In: Vehicle System Dynamics, 51 (2013) 7, DOI 10.1080/00423114.2013.793365, pp. 1059–1090.

[Str12] Strecker, W.
Einsatz am Limit, Prüfung sicherheitsrelevanter Bauteile an Fahrrädern
In: Konstruktion (, 2012) 11-12.

List of Tables

List of Figures